A Trajectory-Driven SISO mm-Wave Channel Model for a Human Activity Recognition

Nurilla Avazov, Rym Hicheri, Matthias Pätzold,
Faculty of Engineering and Science, University of Agder, P.O.Box 509, 4898 Grimstad, Norway
E-mails: {nurilla.avazov, rym.hicheri, matthias.paetzold}@uia.no

***Abstract*—In this paper, we propose a trajectory-driven three-dimensional (3D) non-stationary channel model for millimeter wave (mm-Wave) single-input single-output (SISO) systems. The proposed channel model is designed to model and simulate the micro-Doppler characteristics of human walking activities in indoor environments. We present an expression of the time-variant (TV) channel transfer function (CTF), where its temporal variation is determined by the trajectories of moving human body segments. As moving human body segments, we study the influence of the head, chest, and hips. We investigate the TV Doppler characteristics of the proposed channel caused by the motion of the person. To do so, we focus on the TV spectrogram and the TV mean Doppler shift. To confirm the validity of the proposed channel model, we conducted a measurement campaign for human walking activities by using the Ancortek 2400T2R4 software defined radar kit operating at 24 GHz. The TV trajectories of human body segments are collected during the experiment by using the Rokoko smartsuit. The results for the micro-Doppler signature obtained from the measurements are compared with those of the trajectory-driven channel model. The findings show a good match between the proposed channel model and the real-world measurements.**

***Index Terms*—Mean Doppler shift, mm-Wave propagation, radar, spectrogram, time-variant channel models.**

I. Introduction

According to the World Health Organization (WHO), the global population over 60 is expected to double by 2050 [1]. This study also shows that one out of three persons over the age of 60 suffers a fall at least twice a year. These facts challenge healthcare services to adapt to an aging population and advances in new technologies. This is crucial, especially given the growing proportion of the elderly population want to live independently in their homes [2].

In recent years, human activity recognition (HAR) systems have gained considerable attention from both research institutes and healthcare industries. Existing fall detection systems can be categorized into three major groups, such as sensor-based systems [3]–[5], computer vision-based systems [6], and radio-frequency (RF)-based systems [7]–[9]. As was pointed out in [9], RF-based systems have many advantages, which includes privacy ensurence, cost efficiency, and better coverage, when compared to the other two sensing technologies. In addition, RF-based HAR systems do not require wearable devices or direct user involvement with the system. For this reason, we focus in this paper on HAR systems which utilize RF techniques. Such methods extract the information from radio signals scattered from the user's body in a home environment.

In this context, several RF-based HAR systems have been proposed in the literature [10]–[14]. Ding et al. [11] proposed a dynamic range-Doppler model for detecting various human activities, such as falling, stepping, jumping, walking, squatting, and jogging. They analyzed the range-Doppler and radar cross-section characteristics by using a frequency-modulated continuous wave (FMCW) radar system. In [12], a hands-free HAR system was proposed using millimeter wave (mm-Wave) sensors, where the recorded data allows the replication of human activity based on the motions of body segments. In [14], Cheng et al. have investigated measurement-based fall detection systems and evaluated the performance of various deep learning methods to classify fall activities. They concluded that long-term training of classifiers is required, which is one of the drawbacks to be solved. The survey in [15] reviewed channel state information (CSI)-based indoor positioning systems to provide accurate location services. In [16], a micro-Doppler signature-based analysis of a hand trajectory has been presented. They extracted the hand motion profile from the information contained in the received Doppler signature of wireless communication links.

According to the aforementioned references, channel models, which can accurately describe the impact of indoor human activities on the Doppler characteristics are essential to design efficient HAR systems. In this context, a 3D trajectory-driven non-stationary channel model has been proposed in [17], where the space-time correlation functions of the underlying channel were studied under non-isotropic scattering conditions. Later, Zheng et al. proposed a Wi-Fi-based recognition system to estimate the velocity profiles of different gestures in [18]. It was found that the proposed method is scenario dependent and can hardly be generalized.

When a person is performing an activity, the motion of the different human body segments introduces changes in Doppler properties of the underlying non-stationary channel. In this regard, analysing these TV Doppler effects allows us to detect various daily activities, such as walking, sitting, falling, and eating. More studies on this topic can be found in [9], [11]. Traditionally, this task can be achieved through the investigation of the spectrogram and the TV mean Doppler shift of the channel [2], [19], [20]. Therefore, designing a generic analytical propagation model that takes into account the TV Doppler characteristics caused by moving body segments is of great importance. Specifically, such models enable to get a deeper insight into the individual contribution of distinct body

978-1-6654-2854-5/21/$31.00 ©2021 IEEE

segments using their TV trajectories.

The review of the literature shows that, to the best of the authors' knowledge, existing channel models do not properly incorporate the non-stationary behavior of distinct human body segments in indoor environments. Therefore, this paper focuses on the analysis of a trajectory-driven channel model for single-input single-output (SISO) radar systems operating the mm-Wave frequency band. Here, we consider a moving person, which is modelled by a cluster of moving point scatterers. Each moving point scatterer represents the center of mass (CoM) of a body segment described by a TV trajectory. The trajectories of the cluster of point scatterers are the inputs of the proposed trajectory-driven channel model. Expressions for the TV channel transfer function (TV-CTF) and the complex channel gains are presented. The corresponding Doppler characteristics in form of the TV spectrogram and the TV mean Doppler shift are analyzed. To validate the proposed model, we conducted a real-world measurement campaign by using a mm-Wave radar kit (Ancortek SDR-KIT 2400T2R4) in an indoor environment. As an example of a human activity, we consider a walking scenario. To obtain the TV trajectories of the person's body segments, such as head, chest, and hips, we use the Rokoko smartsuit [21]. To assess the performance of the proposed model, we compare the TV spectrogram of the measured RF data with that of the trajectory-driven channel model. The results of the spectrogram analysis ascertain a good agreement between the measurements and simulation.

The organization of the paper is as follows. Section II describes the investigated scenario. Section III presents the proposed trajectory-driven SISO channel model. The Doppler analysis is addressed in Section IV. Measurement and simulation results are reported in Section V. Finally, Section VI concludes the paper.

II. 3D Geometrical Indoor Channel Model

The 3D non-stationary indoor wave propagation scenario investigated in this paper is illustrated in Fig. 1. For our analysis, we consider a SISO radar system, consisting of a single transmitter antenna A^T and a receiver antenna A^R. The antennas A^T and A^R are located at the fixed positions (x^T, y^T, z^T) and (x^R, y^R, z^R), respectively. Moreover, a person is moving in the indoor space. This person is modelled by N moving point scatterers S_n^M, $n = 1, 2, \ldots, N$. Here, the point scatterer S_n^M describes the CoM of the nth human body segment, which is represented by a red disc (●). The TV position of the nth moving point scatterer S_n^M is described by the TV coordinates $x_n^M(t)$, $y_n^M(t)$, and $z_n^M(t)$. We denote the TV trajectory of S_n^M as $\mathcal{C}_n(t) = (x_n^M(t), y_n^M(t), z_n^M(t))$. The TV Euclidean distance $d_n^T(t)$ between the transmitter antenna A^T and the nth moving scatterer S_n^M can be expressed in terms of the TV coordinates $x_n^M(t)$, $y_n^M(t)$, and $z_n^M(t)$ as

$$d_n^T(t) = \sqrt{(x_n^M(t) - x^T)^2 + (y_n^M(t) - y^T)^2 + (z_n^M(t) - z^T)^2}. \tag{1}$$

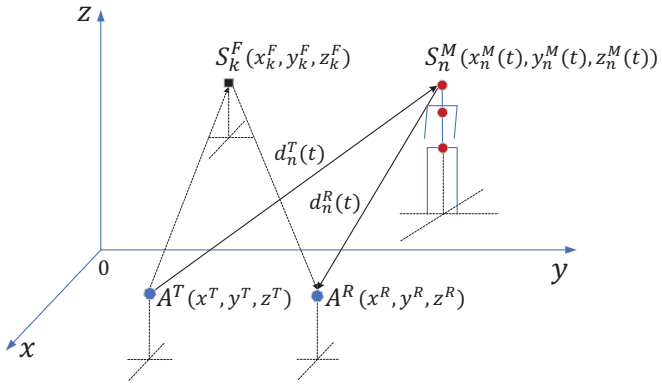

Fig. 1. 3D geometrical model for a SISO radar system with M moving point scatterers S_n^M $(n = 1, 2, \ldots, N)$ and K fixed scatterers S_k^F $(k = 1, 2, \ldots, K)$.

Similarly, the TV Euclidean distance $d_n^R(t)$ between the nth moving scatterer S_n^M and the receiver antenna A^R can be computed as follows

$$d_n^R(t) = \sqrt{(x_n^M(t) - x^R)^2 + (y_n^M(t) - y^R)^2 + (z_n^M(t) - z^R)^2}. \tag{2}$$

There are several fixed objects in the room such as furniture, decoration items, and walls. These objects are modelled by K fixed point scatterers S_k^F $(k = 1, 2, \ldots, K)$. Each fixed scatterer S_k^F has a fixed position (x_k^F, y_k^F, z_k^F).

In the following, we investigate a 3D non-stationary indoor channel model that is driven by the TV trajectories $\mathcal{C}_n(t)$ of the body segments (moving point scatterers S_n^M).

III. Channel Model

In this section, we present the TV-CTF of a SISO channel. As depicted in Fig. 1, the radio signal propagates from the transmitter antenna A^T to the mobile scatterers S_n^M and fixed scatterers S_k^F, respectively, and impinges at the receiver antenna A^R. The TV-CTF of the link from A^T to A^R can be expressed as:

$$H(t, f') = \sum_{n=1}^{N} H_n^M(t, f') + \sum_{k=1}^{K} H_k^F(f') \tag{3}$$

where $H_n^M(t, f')$ and $H_k^F(f')$ stand for the complex TV-CTF corresponding to the nth moving scatterer S_n^M and the kth fixed scatterer S_k^F, respectively. From (3), we can see that the terms $H_n^M(t, f')$ $(n = 1, 2, \ldots, N)$ are TV, while the terms $H_k^F(f')$ $(k = 1, 2, \ldots, K)$ are time invariant. The first (second) term of the TV-CTF $H(t, f')$ in (3) can be presented as a superposition of N (K) components caused by mobile (fixed) scatterers. ACcording to [22], the nth and kth terms of the complex TV-CTFs $H_n^M(t, f')$ and $H_k^F(f')$ can be presented as

$$H_n^M(t, f') = c_n^M(t) e^{j[\theta_n^M - 2\pi(f' + f_c)\tau_n'^M(t)]} \tag{4}$$

and

$$H_k^F(f') = c_k^F e^{j[\theta_k^F - 2\pi(f' + f_c)\tau_k'^F]} \tag{5}$$

respectively. The symbol f_c stands for the center carrier frequency. In (4), the nth component of the TV-CTF $H_n^M(t, f')$ associated with the nth moving scatterer S_n^M takes into account a TV path gain $c_n^M(t)$, a constant initial phase θ_n^M, and a TV propagation delay $\tau_n^{'M}(t)$. Based on the free-space path-loss model, the TV path gain $c_n^M(t)$ of S_n^M can be expressed as [23]

$$c_n^M(t) = a_n[d_n^T(t) \cdot d_n^R(t)]^{-\gamma/2} \tag{6}$$

where a_n is a parameter that depends on the radar transmit/receive antenna gain, wave length, and the transmission power. The symbol γ is the path-loss exponent. The TV propagation delay $\tau_n^{'M}(t)$ of the radio signal travelling from A^T to A^R via the nth moving scatterer S_n^M can be obtained by using the Euclidean distances $d_n^T(t)$ and d_n^R as:

$$\tau_n^{'M}(t) \quad = \quad \frac{d_n^T(t) + d_n^R(t)}{c_0} \tag{7}$$

where c_0 represents the speed of light. It is obvious that the TV propagation delays $\tau_n^{'M}(t)$ are determined by using the TV trajectories $\mathcal{C}_n(t) = (x_n^M(t), y_n^M(t), z_n^M(t))$ via the TV radial distances given in (1) and (2).

Analogously, the kth component of the CTF $H_k^F(f')$ corresponding to the fixed kth scatterer is defined by the constant path gain c_k^F, constant phase θ_k^F, and constant propagation delay $\tau_k^{'F}$. In this model, we assume that both phases θ_n^M and θ_k^F are modelled as independent and identically distributed (i.i.d.) random variables, where each of them is uniformly distributed over the interval between $-\pi$ and π.

In this paper, our primarily focus is to investigate the impact of moving scatterers (body segments) on the TV Doppler characteristics of the 3D non-stationary indoor channel. In this regards, we apply high-pass filtering to mitigate the contribution of the fixed scatterers (objects) to the overall propagation phenomenon. Hence, the second term of (3) will be neglected in the following analysis.

IV. Spectrogram Analysis

This section presents the spectrogram capturing the effects of the body segments of a moving person in an indoor environment. In our analysis, we compute the spectrogram and the corresponding TV mean Doppler shift. The spectrogram associated with the propagation link between A^T and A^R is represented by $S(f, t)$.

To determine the spectrogram $S(f, t)$, we first need to compute the channel impulse response $h(t, \tau')$ by taking the inverse Fourier transform (IFFT) of the complex CTF $H(t, f')$ with respect to frequency f'. Then, by integrating the channel impulse response $h(t, \tau')$ over delay τ' from 0 to the maximum propagation delay $\tau'_{\max}$, we obtain the following solution of the complex channel gain $\mu(t)$ [24, Eq. (14)]

$$\mu(t) = \sum_{n=1}^{N} c_n^M(t) e^{j\left[\theta_m^M - 2\pi f_c \tau_n^{'M}(t)\right]}. \tag{8}$$

The spectrogram $S(f, t)$ is equal to the squared value of the short-time Fourier transform (STFT) $X(f, t)$, i.e.,

$$S(f, t) = |X(f, t)|^2 \tag{9}$$

where the STFT $X(f, t)$ is defined as

$$X(f, t) = \int_{-\infty}^{\infty} \mu(t) w(t' - t) e^{-i2\pi f t'} dt'. \tag{10}$$

In (10), $w(t)$ is a window function.

The TV mean Doppler frequency $B_{\mu_{i,j}}^{(1)}(t)$ is defined as the first-order moment of the spectrogram $S(f, t)$ and can be obtained according to [22]

$$B_\mu^{(1)}(t) = \frac{\int_{-\infty}^{\infty} f S(f, t) df}{\int_{-\infty}^{\infty} S(f, t) df}. \tag{11}$$

V. Measurement and Simulation Results

This section presents the measurement campaign and simulation results for the Doppler characteristics influenced by a walking person. Since walking is one of our mostly performed daily activities, we consider this in our experiment. The measurement campaign was carried out in an indoor environment as illustrated in Fig. 2. Compared to the analysis presented in [25], where the impact of the antenna positions has been investigated, the current study aims at validating the proposed trajectory-driven channel model for human activity recognition. For this reason, we consider a SISO communication system with collocated antennas. In this regard, for the measurement campaign, we use the Ancortek SDR-KIT 2400T2R4 radar system operating at the 24 GHz frequency band in SISO mode. The radar kit transmits chirp signals with 1 ms chirp duration and 250 MHz bandwidth. The transmitter and the receiver antennas are collocated and placed at a height of 1.1 m as depicted in Fig. 2.

In our experiment, we also use the Rokoko smartsuit [21], which has 19 sensors attached to it that allow us to record the trajectories of human body segments, e.g., head, chest, hips, lower/upper arms, and lower/upper thighs. The radar system is located in a corridor of 10 m length, 3.8 m width, and 2.5 m height. The person moves 4.6 m away from the radar system, makes a U-turn, and then walks back toward the radar system. The sensors of the Rokoko smartsuit are connected to a main hub. To record and store the trajectory data, the main hub transmits the collected data to the Rokoko Studio software [21] via a WiFi connection (see Fig. 2). The recorded data can be analyzed and processed by animating the avatar or skeleton of the person. Figure 3 shows the walking person, the corresponding avatar, and its skeleton obtained from the Rokoko studio software. Finally, the received trajectory data can be exported in various file formats, such as FBX[1], BVH[2],

[1]Filmbox.
[2]Bounding volume hierarchy.

Fig. 2. Measurement setup for collecting RF sensing data and the trajectories of body segments during human walking experiment.

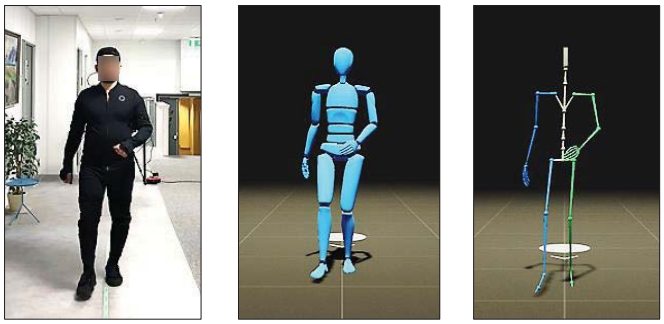

(a) (b) (c)

Fig. 3. Illustration of (a) the walking person, (b) avatar, and (c) skeleton of the avatar.

and CSV[3]. For our analysis, we used the BVH file format that contains the trajectory information (x, y, z positions) of each body segment and its corresponding time stamps.

In this specific scenario, we observed that the main body segments influencing the Doppler phenomenon are the head, chest, and hips. The effects of these body segments on the Doppler characteristics of the indoor non-stationary channel model are therefore the focus of the following analysis.

The TV trajectories along the x-axis, y-axis, and z-axis of the head, chest, and hips of the moving person are illustrated in Figs. 4−6, respectively. Figure 4 shows that the person walked a distance of approximately 4.8 m. It is also interesting to see that the TV trajectories $x_1(t)$, $x_2(t)$, and $x_3(t)$ of the head, chest, and hips, respectively, are almost identical. However, Fig. 5 demonstrates a small drift in the direction of the y-displacement. According to the manufacturer of the smartsuit [26], this can be the result of the impact of the electromagnetic field surrounding the sensors. Therefore, it is critical to operate in a magnetic safe zone when using the smartsuit. Finally, we can see that the z-displacements of the head, chest, and hips are

[3]Comma-separated values.

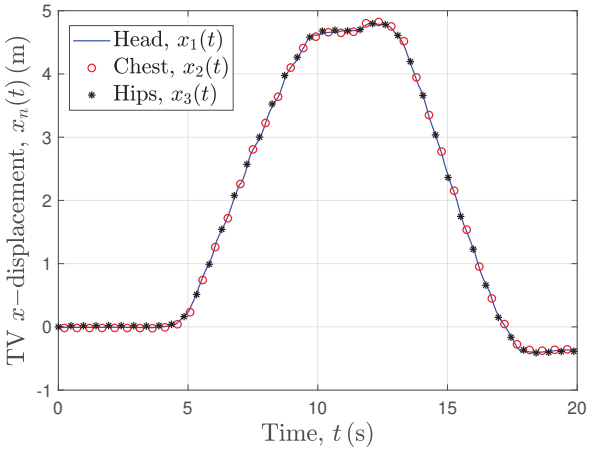

Fig. 4. TV x-displacement $x_n(t)$ of human body segments: head ($n = 1$), chest ($n = 2$), and hips ($n = 3$).

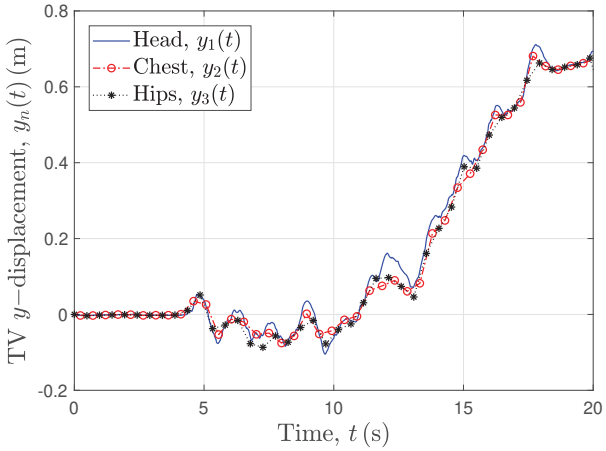

Fig. 5. TV y-displacement $y_n(t)$ of human body segments: head ($n = 1$), chest ($n = 2$), and hips ($n = 3$).

well captured as shown in Fig. 6. It is noteworthy to mention that the results in Fig. 6 are in accordance with the position of the sensors with respect to the height of the walking person. This confirms the validity of the recorded trajectory data. The sinusoidal fluctuation of the z-displacement corresponds to the walking activity, which is in accordance with the results reported in [27]. From the results illustrated in Figs. 4−6, we can also track the person's walking activity. For example, at the beginning of the recording, the person does not move, which is translated by time-invariant displacements for a period of almost 4.8 s. Then, the person starts walking away from the radar kit for about 4.8 m and stops to make a U-turn to return to the radar kit. The U-turn motion takes approximately 3 s (seen between 10 s and 13 s). Finally, the person returns to the radar kit, which takes 5 s and is almost equal to the time it takes to walk walk away from the radar unit.

Next, we compute the spectrogram of the complex channel gain by following the steps described in (8)–(10). Without loss of generality, we set $a_n = 1/\sqrt{N}$. Figs. 7(a) and (b) depict

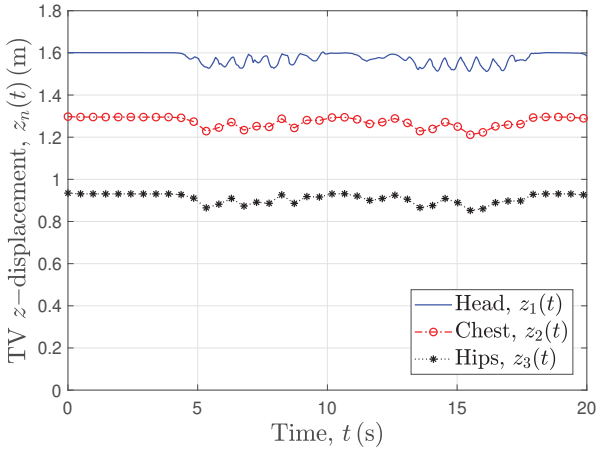

Fig. 6. TV z-displacement $z_n(t)$ of human body segments: head ($n = 1$), chest ($n = 2$), and hips ($n = 3$).

the spectrogram $S^{\star}(f,t)$ of the measured received radar signal and the spectrogram $S(f,t)$ of the trajectory-driven simulation model, respectively. A good match can be observed between both spectrograms $S^{\star}(f,t)$ and $S(f,t)$. This reflects the similar walking patterns shown in Figs. 4–6. For example, when the person walks away from the radar system, we see negative TV Doppler frequencies in the spectrograms. By contrast, going towards the antennas results in positive TV Doppler frequencies. In addition, the same number of walking steps corresponding to the number of peaks can be counted from both spectrograms $S^{\star}(f,t)$ and $S(f,t)$.

Fig. 8 illustrates the TV mean Doppler shift $B_{\mu}^{(1)\star}(t)$ of the measured received radar signal together with the TV mean Doppler shift $B_{\mu}^{(1)}(t)$ of the trajectory-driven simulation model. Overall, there is a good agreement between the measured and simulated TV mean Doppler shifts. However, it should be noted that the quality of the fit degrades during the observation time between 13 s and 20 s. This can be explained by the fact that the displacement along the $y-$axis experiences a drift during the same time intervals (see Fig. 5). Note that this drift does not impact the overall trend of the TV mean Doppler shift.

VI. Conclusion

In this paper, we have proposed a non-stationary indoor trajectory-driven channel model for HAR systems in the presence of a moving person. The dominating body segments have been modelled by a cluster of moving point scatterers. In this regard, we have presented expressions for the TV-CTF and the complex channel gain, where the inputs are the TV trajectories of human body segments. We have investigated the TV Doppler characteristics of the proposed trajectory-driven channel model. The validity of the proposed model has been confirmed by real-world measurement data collected during a walking scenario. The RF data has been collected utilizing a SISO radar kit operating at 24 GHz. The novelty of this paper is that the TV trajectories of the body segments have been obtained by means of the Rokoko smartsuit. Then, these

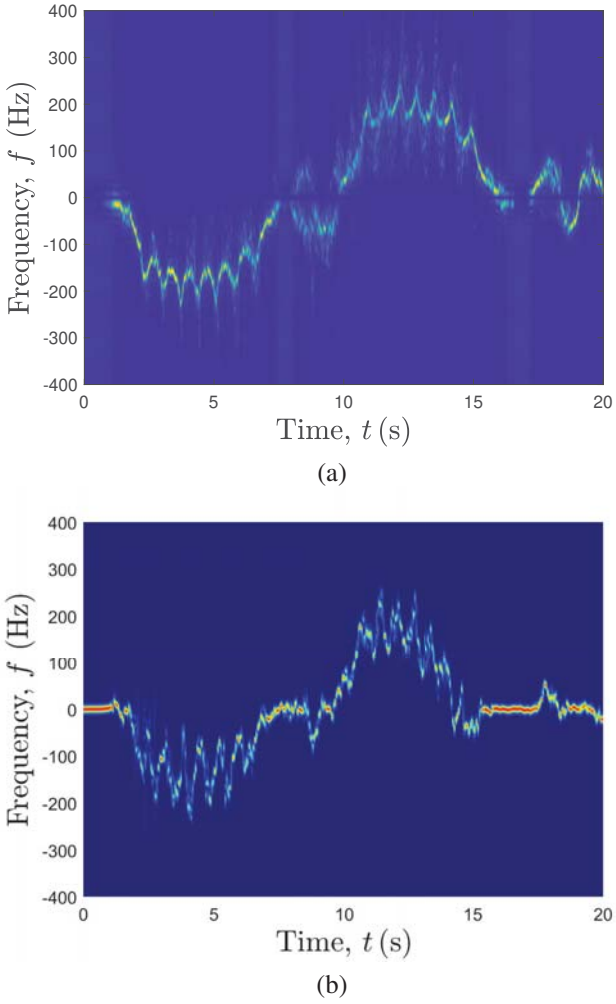

Fig. 7. (a) TV spectrogram $S^{\star}(f,t)$ of the measured received radar signal and (b) TV spectrogram $S(f,t)$ of the trajectory-driven simulation model.

trajectories have been fed to the channel model. A comparison between the Doppler properties of the measured RF signals and those corresponding to the trajectory-driven channel model has been performed for a forward/backward walking scenario. The results demonstrate a good agreement between the Doppler characteristics of the measured data and those of the proposed method. It has been found that the presence of a drift in the TV trajectories impacts the resulting Doppler properties. Therefore, it is important to consider the effect of drifts when evaluating the performance of sensor-based systems. This work can serve as a basis for analyzing more complex indoor activities for future real-life applications, such as remote healthcare and independent living.

Acknowledgment

This work has been carried out within the scope of the CareWell project funded by the Research Council of Norway under the grant number 300638/O70.

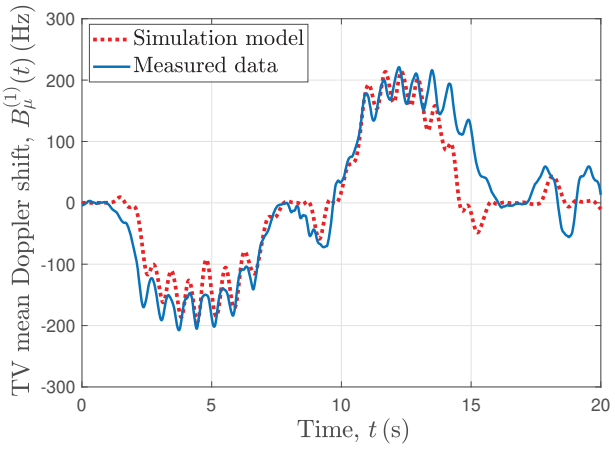

Fig. 8. Comparison of the TV mean Doppler shift $B_\mu^{(1)}(t)$ of the trajectory-driven simulation model and that obtained from the measured received radar signal.

REFERENCES

[1] "WHO Global report on falls prevention in older age," *Dept. Ageing Life Course, Geneva, Switzerland*, 2007.

[2] M. G. Amin, Y. D. Zhang, F. Ahmad, and K. C. D. Ho, "Radar signal processing for elderly fall detection: The future for in-home monitoring," *IEEE Signal Process. Mag.*, vol. 33, no. 2, pp. 71–80, 2016.

[3] D. M. Karantonis, M. R. Narayanan, M. Mathie, N. H. Lovell, and B. G. Celler, "Implementation of a real-time human movement classifier using a triaxial accelerometer for ambulatory monitoring," *IEEE Trans. Inf. Technol. Biomed.*, vol. 10, no. 1, pp. 156–167, 2006.

[4] D. Tao, L. Jin, Y. Yuan, and Y. Xue, "Ensemble manifold rank preserving for acceleration-based human activity recognition," *IEEE Trans. Neural Netw. Learn. Syst.*, vol. 27, no. 6, pp. 1392–1404, 2016.

[5] A. Wang, G. Chen, J. Yang, S. Zhao, and C. Chang, "A comparative study on human activity recognition using inertial sensors in a smartphone," *IEEE Sensors J.*, vol. 16, no. 11, pp. 4566–4578, 2016.

[6] S. Zhang, Z. Wei, J. Nie, L. Huang, S. Wang, and Z. Li, "A review on human activity recognition using vision-based method," *J. Healthcare Eng.*, 2017.

[7] H. Fei, F. Xiao, J. Han, H. Huang, and L. Sun, "Multi-variations activity based gaits recognition using commodity WiFi," *IEEE Trans. Veh. Tech.*, vol. 69, no. 2, pp. 2263–2273, 2020.

[8] Y. Peng and S. Guo, "Detailed feature representation and analysis of low frequency UWB radar range profile for improving through-wall human activity recognition," in *IEEE Radar Conf. (RadarConf'20)*, 2020, pp. 1–6.

[9] J. Liu, H. Liu, Y. Chen, Y. Wang, and C. Wang, "Wireless sensing for human activity: A survey," *IEEE Commun. Surveys Tut.*, vol. 22, no. 3, pp. 1629–1645, 2020.

[10] S. Wang and G. Zhou, "A review on radio based activity recognition," *Digit. Commun. and Netwo.*, vol. 1, no. 1, pp. 20–29, 2015.

[11] C. Ding *et al.*, "Continuous human motion recognition with a dynamic range-Doppler trajectory method based on FMCW radar," *IEEE Trans. Geosci. Remote Sens.*, vol. 57, no. 9, pp. 6821–6831, 2019.

[12] S. M. Kwon *et al.*, "Demo: Hands-free human activity recognition using millimeter-wave sensors," in *IEEE Int. Symp. on Dynamic Spectrum Access Netw. (DySPAN'19)*, 2019, pp. 1–2.

[13] J. Ding and Y. Wang, "A WiFi-based smart home fall detection system using recurrent neural network," *IEEE Trans. Consumer Electron.*, vol. 66, no. 4, pp. 308–317, 2020.

[14] H. Cheng, J. Zhang, Y. Gao, and X. Hei, "Deep learning Wi-Fi channel state information for fall detection," in *IEEE Int. Conf. on Consumer Electron. - Taiwan (ICCE-TW'19)*, 2019, pp. 1–2.

[15] W. Liu *et al.*, "Survey on CSI-based indoor positioning systems and recent advances," in *Int. Conf. on Indoor Positioning and Indoor Navig. (IPIN'19)*, 2019, pp. 1–8.

[16] N. Keerativoranan, P. Hanpinitsak, K. Saito, and J. I. Takada, "Analysis of non-intrusive hand trajectory tracking by utilizing micro-Doppler signature obtained from Wi-Fi channel state information," *IEEE Access*, vol. 8, pp. 176 430–176 444, 2020.

[17] Q. Z. et al., "Spatial correlations of a 3-D non-stationary MIMO channel model with 3-D antenna arrays and 3-D arbitrary trajectories," *IEEE Wireless Commun. Lett.*, vol. 8, no. 2, pp. 512–515, 2019.

[18] Z. et al., "Zero-effort cross-domain gesture recognition with Wi-Fi," in *Proceedings of the 17th Annual Int. Conf. on Mobile Syst., Appl., and Services*, ser. MobiSys'19. New York, NY, USA: Association for Computing Machinery, 2019, pp. 313–325. [Online]. Available: https://doi.org/10.1145/3307334.3326081

[19] V. C. Chen, F. Li, S. . Ho, and H. Wechsler, "Micro-Doppler effect in radar: phenomenon, model, and simulation study," *IEEE Trans. Aero. and Electron. Syst.*, vol. 42, no. 1, pp. 2–21, 2006.

[20] M. Wu, X. Dai, Y. D. Zhang, B. Davidson, M. G. Amin, and J. Zhang, "Fall detection based on sequential modeling of radar signal time-frequency features," in *IEEE Int. Conf. on Healthcare Inform.*, Sep. 2013, pp. 169–174.

[21] "The Rokoko Smartsuit Pro," [Online], Available: www.rokoko.com. Last visited in June, 2021.

[22] A. Abdelgawwad, A. Borhani, and M. Pätzold, "Modelling, analysis, and simulation of the micro-Doppler effect in wideband indoor channels with confirmation through pendulum experiments," *MDPI, Sensors*, vol. 20, no. 4, pp. 1–18, Feb. 2020.

[23] R. Hicheri, A. Abdelgawwad, and M. Pätzold, "A non-stationary relay-based 3D MIMO channel model with time-variant path gains for human activity recognition in indoor environments," *Annals of Telecommun.*, pp. 1–11, 2021.

[24] R. Hicheri, N. Avazov, M. Muaaz, and M. Pätzold, "The transfer function of non-stationary indoor channels and its relationship to system functions of LFMCW radars," in *IEEE International Workshop on Signal Processing Advances in Wireless Communications*, 2021, Accepted.

[25] N. Avazov, R. Hicheri, and M. Pätzold, "A trajectory-driven SIMO mm-wave channel model for a moving point scatterer," in *2021 15th European Conference on Antennas and Propagation (EuCAP)*, 2021, pp. 1–5.

[26] "The Rokoko Smartsuit Pro: Help and Community," [Online], Available: https://help.rokoko.com/support/solutions/articles/47001095035-getting-started-guide-smartsuit-promotion-capture-stage-considerations-0-4. Last visited in August, 2021.

[27] S.-U. Jung and M. S. Nixon, "Estimation of 3D head region using gait motion for surveillance video," in *4th International Conference on Imaging for Crime Detection and Prevention 2011 (ICDP 2011)*, 2011, pp. 1–6.